Artificial Neural Network-Based Adaptive Voltage Regulation in Distribution Systems using Data-Driven Stochastic Optimization

Krishna Sandeep Ayyagari, Reynaldo Gonzalez, Yufang Jin, Miltiadis Alamaniotis
Sara Ahmed and Nikolaos Gatsis

***Abstract*— Modern distribution networks have a high integration level of distributed energy resources (DERs). Due to the stochastic nature of renewable energy production and user load consumption, it is challenging for distribution system operators (DSOs) to maintain the voltages within safe bounds. Centralized, decentralized, and distributed operational schemes have been used to tackle these challenges, however centralized and distributed methods require extensive communication infrastructure. This paper utilizes an offline, centralized data-driven conservative convex approximation of chance constrained optimal power flow to compute PV inverter reactive power set-points with consideration of PV and load uncertainties. Then, an artificial neural network (ANN) controller is developed for each PV inverter in order to mimic the centralized PV inverter control set-points, in a decentralized fashion. Numerical tests using real-world data on a benchmark feeder demonstrate that ANN controllers can attain near-optimal performance in voltage regulation and loss improvements while satisfying the probabilistic constraints.**

***Index Terms*— Chance constraints; distributed energy resources; distribution system; voltage regulation; artificial intelligence; neural network; converter control; data-driven control design.**

I. Introduction

Voltage regulation in power distribution systems is usually accomplished by legacy switched-type devices such as capacitors, load tap changers, and step voltage regulators, which operate at slower pace [1], and more recently, by fast-responding distributed energy resources (DERs). Due to the increased penetration of DERs, distribution systems have seen an increase in power flow and voltage variability, posing new challenges to the DSO. Recent amendments of the IEEE 1547-2018 Standard [2], have now allowed PV inverters to provide reactive power support for voltage regulation.

Earlier efforts to address the voltage regulation problem in distribution networks aimed at developing PV inverter control which utilizes optimal power flow (OPF) in a centralized, decentralized, or distributed communication framework to infer the optimal set-points of all the inverters; see e.g., [3]–[12]. A centralized framework minimizes the operating cost, although it requires extensive monitoring and communication infrastructure for system-wide optimal operation. Decentralized control strategies, on the other hand, require no communication and only use local information to modify the DERs behavior. Distributed approaches use limited communication between neighboring DERs to achieve close-to-optimal operation, however these method are susceptible to communication delays and errors.

There is an abundance of readily available historic data from utility smart meters that are being installed as a part of the transition to the smart grid [13]. A newer approach, which has been attaining more popularity in recent years, is data-driven voltage regulation for DERs using machine learning methods [14]–[21].

A. Approach and contributions

This paper utilizes a data-driven conservative approximation of chance constraints accounting for PV generation and load uncertainty using the conditional value at risk (CVaR) [22]–[25] which does not require any assumptions on the distribution. It significantly extends the previous work in [15], which achieves voltage regulation through regression-based inverter control. Subsequently, this paper develops an artificial neural network (ANN) based controller that can be used for real-time control of PV inverters in distribution networks to achieve network-wide optimal operation while having no communication requirements (decentralized operation). The main advantage of the ANN-based controller over a regression-based controller is that the ANN-based controller are generally model free which can account for any degree of non-linearity [26]. Also, ANNs can easily model noisy data from smart energy meters as they are fault-tolerant, noise immune and robust in nature. This paper compares the performance of the proposed ANN-based controller against the existing regression-based control benchmark in [15] with respect to thermal loss minimization and voltage regulation calculated by a non-linear power flow method (Z-bus method) [27] using real-world data on the IEEE 13-node distribution network.

The remainder of the paper is organized as follows. The

The authors are with the Department of Electrical and Computer Engineering at the University of Texas at San Antonio, San Antonio, TX 78249, USA. Email:{krishnasandeep.ayyagari, reynaldo.gonzalez, yufang.jin, miltos.alamaniotis, sara.ahmed, nikolaos.gatsis}@utsa.edu. This material is based upon work supported by the National Science Foundation under Grant No. ECCS-1847125.

978-1-7281-0395-2/19/$31.00 ©2019 IEEE

network and resource models are introduced in Section II. Section II also discusses the voltage regulation problem with generic chance constraints and their data driven approximations. Section III includes the network setup and the process of collecting training and test data. Section IV explains the ANN structure. Section V compares the performance of ANN based controllers with regression. Finally, conclusions are drawn in section VI.

II. System Model and Centralized Stochastic Optimal Power Flow (SOPF)

In this section, we provide the network and resource model adopted in this work. Subsequently, we describe the problem of accounting for the uncertainty in user load and PV generation using a conservative convex approximation of chance constraints. The overall optimization problem consists of the objective function and constraints which are essential in finding the globally optimal DER set-points and will in turn influence the design of local controllers.

A. Grid model

A single-feeder radial distribution grid consisting of $N+1$ buses and N lines is modeled by a tree graph[1]. Let $\mathcal{N}_0 := \{0,\dots,N\}$ denote the set of all nodes, and $L := \{1,\dots,N\}$ the set of lines. The substation bus (root node) is indexed as node 0 and connects the feeder to the transmission network. All non-substation nodes comprising $\mathcal{N} := \{1,\dots,N\}$ represent user buses. Let $\mathcal{C}_n$ denote the set of children buses related to bus n, and π_n the parent of bus n.

Let v_n denote the squared voltage magnitude of bus $n \in \mathcal{N}_0$, and let $s_n = p_n + jq_n$ denote the complex power injected into bus n. For each line $n \in L$, let $z_n = r_n + jx_n$ denote its series impedance, and $S_n = P_n + jQ_n$ the power flowing from the sending bus π_n into node n. The squared voltage magnitude at the substation v_0 is known and fixed. We adopt the linearized distribution flow (LDF) model [28]:

$$P_n = \sum_{k\in\mathcal{C}_n} P_k - p_n \tag{1}$$

$$Q_n = \sum_{k\in\mathcal{C}_n} Q_k - q_n - b_n^{\rm sh} v_n \tag{2}$$

$$v_n = v_{\pi_n} - 2\ \mathrm{Re}[z_n^* S_n] \tag{3}$$

where $b_n^{\rm sh}$ is the susceptance between bus n and the ground and models any shunt capacitor at bus n as well as the shunt admittances of the π-model of the lines incident at bus n. Also, let $\mathbf{A}$ be the reduced branch bus incidence matrix (omitting the slack bus) and $\mathbf{F} := -\mathbf{A}^{-1}$. We define $\mathbf{R} := 2\mathbf{F}\mathrm{diag}(\mathbf{r})\mathbf{F}^\top$, $\mathbf{X} := 2\mathbf{F}\mathrm{diag}(\mathbf{x})\mathbf{F}^\top$, $\mathbf{J} := [\mathbf{I}_N - \tilde{\mathbf{X}}]^{-1}$ and $\tilde{\mathbf{X}} := \mathbf{X}\mathrm{diag}(\mathbf{b}^{\rm sh})$. Eq. (1), (2) and (3) can be written more compactly as $\mathbf{v} = \mathbf{J}(\mathbf{R}\mathbf{p} + \mathbf{X}\mathbf{q} + \mathbf{1}_N v_0)$ which linearly relates power injections $\mathbf{p}$ and $\mathbf{q}$ to the squared voltage magnitudes, and generalizes [29] to include shunt capacitors.

[1]Upper-case (lower-case) boldface is used for matrices (column vectors); $(.)^\top$ for transposition; $(.)^*$ for complex-conjugate, and $(.)^{-1}$ for inverse; Re denotes the real part of a complex number, and $j := \sqrt{-1}$ is the imaginary unit. For a given $N \times 1$ vector $\mathbf{x}$, $\mathrm{diag}(\mathbf{x})$ returns the $N \times N$ matrix with the elements of $\mathbf{x}$ in its diagonal, and $\mathbb{E}$ denotes the expectation operator. Finally, $\mathbf{I}_N$ denotes the $N \times N$ identity matrix; $\mathbf{0}_N$ and $\mathbf{1}_N$ the N dimensional vectors with all zeroes and ones respectively; and $\mathbf{0}_{N\times M}$ is the $N \times M$ matrix with all zeroes.

B. Generation and load model

The network includes $N_{\rm pv}$ distributed PV generators whose connection to the buses is described by the PV-to-node incidence matrix $\mathbf{\Gamma} \in \mathbb{R}^{N\times N_{\rm pv}}$. Due to solar intermittency, the k-th solar generation $p_k^{\rm pv}$ can be modeled as a random variable, while its reactive power injection $q_k^{\rm pv}$ is a control variable. If $S_{k,\max}^{\rm pv}$ is the apparent power capacity for inverter k, its solar generation and reactive injection are constrained by

$$(q_k^{\rm pv})^2 + (p_k^{\rm pv})^2 \le (S_{k,\max}^{\rm pv})^2. \tag{4}$$

The network also includes $N_{\rm c}$ loads (points of consumption) whose connection to the buses is given by the load-to-node incidence matrix $\mathbf{\Psi} \in \mathbb{R}^{N\times N_{\rm c}}$. We model the active and reactive power demand (denoted respectively by $\mathbf{p}^{\rm c}$ and $\mathbf{q}^{\rm c}$) and PV active power generation as random variables. Further, define vector $\mathbf{w} = [\mathbf{p}^{\rm c}, \mathbf{q}^{\rm c}, \mathbf{p}^{\rm pv}]^\top \in \mathbb{R}^{N\times(2N_{\rm c}+N_{\rm pv})}$ as the system disturbance which is uncontrollable and includes the aforementioned random variables.

The active and reactive power injections $\mathbf{p}$ and $\mathbf{q}$ are expressed in terms of controlled input $\mathbf{u}$ and disturbance $\mathbf{w}$ as follows:

$$\mathbf{p} = \mathbf{B}_{\rm w}\mathbf{w} \qquad\qquad \mathbf{q} = \mathbf{\Gamma}\mathbf{u} + \mathbf{K}_{\mathbf{w}}\mathbf{w} \tag{5}$$

where $\mathbf{B}_{\mathbf{w}} = [-\mathbf{\Psi}, \mathbf{0}_{N\times N_{\rm c}}, \mathbf{\Gamma}] \in \mathbb{R}^{N\times(2N_{\rm c}+N_{\rm pv})}$, $\mathbf{u} = [q_1^{\rm pv},\dots,q_{N_{\rm pv}}^{\rm pv}] \in \mathbb{R}^{N_{\rm pv}}$, $\mathbf{K}_{\mathbf{w}} = [\mathbf{0}_{N\times N_{\rm c}}, -\mathbf{\Psi}, \mathbf{0}_{N\times N_{\rm c}}] \in \mathbb{R}^{N\times(2N_{\rm c}+N_{\rm pv})}$. Thus, the squared voltage magnitude $\mathbf{v}$ is expressed as linear function of $\mathbf{u}$ and $\mathbf{w}$ as $\mathbf{v} = (\mathbf{D}\mathbf{u} + \mathbf{E}\mathbf{w} + \tilde{\mathbf{v}}_0)$ with $\mathbf{D} = \mathbf{J}\mathbf{X}\mathbf{\Gamma} \in \mathbb{R}^{N\times N_{\rm pv}}$, $\mathbf{E} = \mathbf{J}(\mathbf{R}\mathbf{B}_{\mathbf{w}} + \mathbf{X}\mathbf{K}_{\mathbf{w}}) \in \mathbb{R}^{N\times(2N_{\rm c}+N_{\rm pv})}$ and $\tilde{\mathbf{v}}_0 = \mathbf{J}\mathbf{1}_N v_0 \in \mathbb{R}^N$.

C. Chance-constrained voltage regulation

The objective is to minimize the thermal losses on the lines, which are approximated by $\sum_{n=1}^N r_n \frac{P_n^2+Q_n^2}{v_0}$ [28]. Furthermore, it can be seen from (5) that $\mathbf{p}$ and $\mathbf{q}$ are linear functions of $\mathbf{u}$ and $\mathbf{w}$. Therefore, thermal losses can be expressed quadratic functions of $\mathbf{u}$ and $\mathbf{w}$ and be given as

$$\begin{aligned}\sum_{n=1}^N r_n \frac{P_n^2+Q_n^2}{v_0} = \frac{1}{2v_0}\Big[&\mathbf{u}^\top\mathbf{R}_{\rm u}\mathbf{u} + \mathbf{w}^\top\mathbf{R}_{\rm w}\mathbf{w} \\ &+ \mathbf{w}^\top\mathbf{R}_{\rm wu}\mathbf{u} + \mathbf{u}^\top\mathbf{R}_{\rm uw}\mathbf{w} + \mathbf{s}_{\rm u}^\top\mathbf{u} \\ &+ \mathbf{s}_{\rm w}^\top\mathbf{w} + h\Big]\end{aligned} \tag{6}$$

for appropriate matrices $\mathbf{R}_{\rm u}$, $\mathbf{R}_{\rm w}$, $\mathbf{R}_{\rm uw}$, $\mathbf{R}_{\rm wu}$, $\mathbf{s}_{\rm u}$, $\mathbf{s}_{\rm w}$ and h.

Since the uncertainty in $\mathbf{w}$ affects the nodal voltages, it is hard to ensure that voltages remain within the bounds dictated by $\mathbf{v}_{\min} \le (\mathbf{D}\mathbf{u} + \mathbf{E}\mathbf{w} + \tilde{\mathbf{v}}_0) \le \mathbf{v}_{\max}$ at all times. Instead, we enforce the latter constraint in a probabilistic fashion. Consider the following optimization problem:

$$\begin{aligned}\text{(P1)}\ \min_{\mathbf{u},\mathbf{v}}\quad &\frac{1}{2v_0}\mathbb{E}\Big[\mathbf{u}^\top\mathbf{R}_{\rm u}\mathbf{u} + \mathbf{w}^\top\mathbf{R}_{\rm w}\mathbf{w} + \mathbf{w}^\top\mathbf{R}_{\rm wu}\mathbf{u} \\ &+ \mathbf{u}^\top\mathbf{R}_{\rm uw}\mathbf{w} + \mathbf{s}_{\rm u}^\top\mathbf{u} + \mathbf{s}_{\rm w}^\top\mathbf{w} + h\Big]\end{aligned} \tag{7a}$$

Fig. 1. Flowchart for Obtaining Results

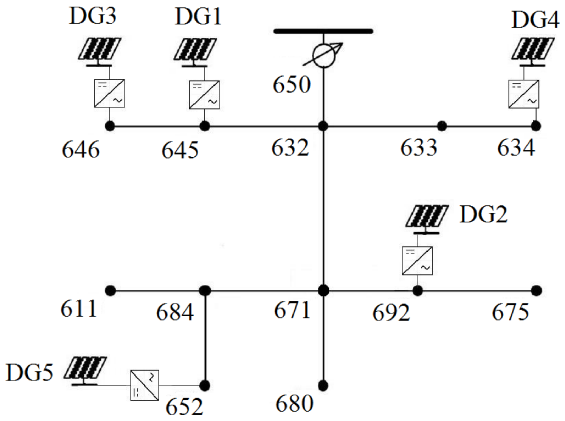

Fig. 2. IEEE-13 Bus Distribution Network with 5 distributed generators (DG)

$$\text{subj. to} \quad \mathbf{v} = \mathbf{D}\mathbf{u} + \mathbf{E}\mathbf{w} + \tilde{\mathbf{v}}_0 \tag{7b}$$

$$\text{Prob}[v_i \geq v_i^{\min}] \geq \alpha_i \tag{7c}$$

$$\text{Prob}[v_i \leq v_i^{\max}] \geq \alpha_i,\ i = 1, \ldots, N \tag{7d}$$

$$|u_k| \leq \sqrt{(S_{\max,k}^{\text{pv}})^2 - (p_k^{\text{pv}})^2},\ k = 1, \ldots, N_{\text{pv}} \tag{7e}$$

It follows from (6) that the dependence of thermal losses on $\mathbf{w}$ render the objective function random. Therefore, the expected value of the losses is minimized. Eq. (7e) may be enforced for all $\mathbf{w}$ (i.e., with probability 1) or probabilistically with a confidence level β_k [30], [31].

In the current formulation (P1), constraints (7c) and (7d) can be problematic for non-Gaussian distributions. In particular, the chance constraints are typically nonconvex [32]. To account for the variety of possible distributions of uncertainty $\mathbf{w}$, a data-driven convex approximation of chance constraint is utilized. Thus, we replace the generic chance constraints in the voltage regulation problem (P1) with CVaR constraints. In particular, the constraints (7b)-(7d) are replaced with $\text{CVaR}_{\alpha_i}[-v_i + v_i^{\min}] \leq 0$ and $\text{CVaR}_{\alpha_i}[v_i - v_i^{\max}] \leq 0$. Also, (7e) is converted to two constraints, and is enforced through the CVaR at level β_k. In addition, a set of scenarios $\{\mathbf{w}_{n_s}\}_{n_s=1}^{N_s}$ (realizations of the random variable $\mathbf{w}$) are assumed to be available. The expected values in the objective of (P1) and in the CVaR constraints are then replaced by their sample average approximations. For the detailed optimization problem refer to [22].

III. Network Setup

This section describes the network being simulated and how the network data is generated for solving the optimization and yielding the training inputs and targets. Additionally, it describes the various simulation scenarios used for comparing results. Each scenario has a different number of training days and test days. A flowchart for obtaining the results in this paper can be seen in Fig. 1.

A. Test feeder and data collection

To analyze the performance of proposed controller design, we use the modified single-phase version of the IEEE 13-node distribution test feeder [33], shown in Fig. 2. The line impedances of the corresponding single-phase version is obtained from [34]. The actual nominal loads per bus from the IEEE 13-node test feeder were divided by three to get the nominal loads for the single-phase version (this is heuristical, since single-phase representation is for balanced networks only). The data used for simulating the network were collected from Pecan Street in Austin, Texas [35]. The Pecan Street organization provides access to a database that records real-world data from 1,115 active homes. Daily consumption (load) and generation (PV) data were obtained for the month of July spanning the years of 2013, 2014, 2015, and 2016. The resolution of data is hourly, giving 24 data points per day. After filtering the homes for complete data for the month of July, a varying number of homes for each year were available to use for load profile generation. Since the dataset contains real power consumption for users, reactive loads were generated by $\mathbf{q}^{\text{c}} = \mathbf{p}^{\text{c}} \tan\phi$ with lagging power factor of 0.9.

The data from each home were used to generate load profiles for nine of the nodes in the distribution network. In order to generate the load profiles, the data for each home were aggregated such that the resulting profile would have one hour out of every day that would equal to a nominal load. Since the data is variable from day-to-day, the nominal load occurs at a random hour for each day. Fig. 3 conceptually illustrates the aggregation of homes into a node. To reduce the correlation between node profiles, a random selection vector was created for each node. Values from the selection vector are used to select random homes from the pool of available home data. Data for each day are added until at least one hour of the day has a cumulative load value that is equal to or greater than the nominal load. As a preliminary step, the number of homes needed is computed for each day in order to meet this requirement. Then, the number of homes needed for each day are averaged and the average number of homes needed for each node are used to generate the final profiles. Thus, the resulting load profiles will on average hit the nominal load value.

The following network nodes are assumed to have PV generation: 646, 645, 634, 652, and 692 as shown in Fig. 2. The same home IDs used to create the load profiles were used

to accumulate generation data for creating the corresponding PV generation profiles.

It should also be noted that data could be obtained from alternate markets or data sets, and be aggregated similarly as the manner above. The resulting network profile aggregations would reflect the market conditions from which the data were obtained. This could be useful for simulating the effects of green markets. Additionally, the aggregation method will work for different network topologies, by using an alternative set of nominal loads. However, the network topology will have to be taken into consideration during the optimization stage.

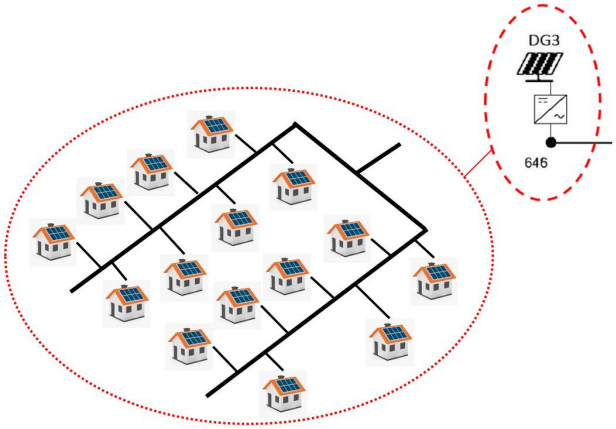

Fig. 3. Illustration showing the aggregation of homes into a node

B. Training and test scenarios

The following training scenarios are used to train and test the efficiency and accuracy of the artificial neural networks and regression models.

- Scenario 1
  - Train from July 3rd to July 27th, 2014
  - Test for July 28th, 2014
- Scenario 2
  - Train for 31 days of July 2015
  - Test for 31 days of July 2016
- Scenario 3
  - Train with 3 months worth of July data (2013, 2014, and 2015)
  - Test for all 31 days of July 2016
- Scenario 4
  - Train with 69 days worth of July weekday data (2013, 2014, and 2015)
  - Test for the first weekdays of July 2016 (Mon. 4th - Fri. 8th)
- Scenario 5
  - Train with 24 days worth of July weekend data (2013, 2014, and 2015)
  - Test for the first weekend of July 2016 (Sat. 2nd - Sun. 3rd)

The first scenario is meant to compare with the results obtained in [22], which has the same number of days for training and testing. This scenario shows the accuracy in same year predictions. The second scenario shows accuracy for year ahead predictions. The third to fifth scenarios use an alternate optimization scheme, where three years worth of July data are optimized in a combined manner, which results in more accurate reactive power set-points. The third scenario shows the results for year-ahead predictions. The fourth scenario considers only weekday data and the fifth scenario considers only weekend data, both again looking at year ahead predictions.

Once the load and generation profiles for all the training scenarios are created, the conservative convex relaxation of stochastic optimization problem (P1) is solved using the CVX toolbox [36] with the Gurobi solver, to yield the optimal reactive power set-points for the training scenarios. The voltage limits $\mathbf{v}_{\min}$ and $\mathbf{v}_{\max}$ are respectively set to 0.95 pu and 1.05 pu as specified by ANSI Standard C84.1. The voltage constraint probability specification and the PV inverter constraint probability specification are set to $\alpha = 0.99$ and $\beta = 0.99$, respectively. The maximum PV penetration $\mathbf{p}^{\text{pv}}_{\max}$ is further assumed to be 80% of the nominal $\mathbf{p}^{\text{c}}$. The maximum apparent power capacity of PV inverter $\mathbf{S}^{\text{pv}}_{\max}$ is assumed to be 105% of $\mathbf{p}^{\text{pv}}_{\max}$ for all the PV inverters. This is assumed for all the training scenarios in the optimization.

To ensure that the control actions respect the physical device limits, the resultant control actions $\mathbf{u}$ obtained from different training scenarios are projected onto their feasible set (in this case, given by eq. (4)) and these projected control actions u^*_{proj} are used as targets to train both the ANN and the regression based controller.

IV. Artificial Neural Network and Regression Benchmark

This section describes the ANN structure as well as the inputs and outputs used for training. It will then explain how the ANN would be implemented into a controller for the inverters which are part of the distribution network. Lastly, it describes the regression technique which was used a benchmark for comparison.

A. ANN structure

An artificial neural network is created for each of the five PV inverters. The ANN was created using the neural network toolbox from MATLAB. The structure of the artificial neural network is a two-layer feed-forward network which can be seen in Fig. 4. The feed-forward network is one of the most widely used neural network structures [37]. The first layer is a hidden layer with sigmoid activation function and ten hidden neurons. The second layer is a linear output layer. This structure is suited for fitting problems, where a data set of numeric inputs is mapped to a set of numeric targets. This works well for this problem because the goal is to map the output of u^*_{proj} to the three input features. The inputs into the neural network of the k-th inverter are net consumption $p^{net}_k = p^{\text{c}}_k - p^{\text{pv}}_k$, reactive power demand q^c_k, and reactive power capacity $q^{\text{c}}_{cap,k} = \sqrt{(S^{\text{pv}}_{\max,k})^2 - (p^{\text{pv}}_k)^2}$ of the PV

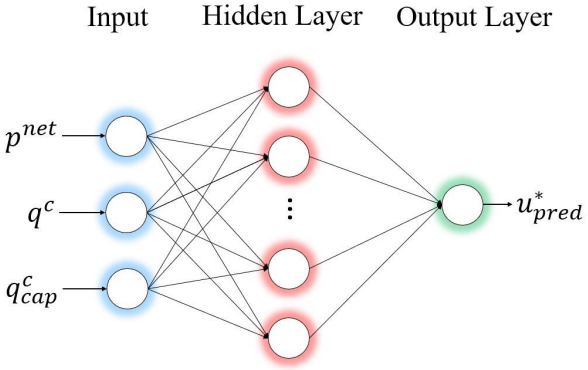

Fig. 4. Artificial Neural Network Structure

inverter. The output of the network is the optimal reactive power set-point for any given combination of the inputs.

B. ANN grid-feeding converter controller

The ANN is part of a proposed grid-feeding converter control system that acts on the distribution network by controlling the amount of reactive power the inverter injects into the network. This type of control is very common for distributed generation systems and is required for operating micro-grids in islanded mode [38]. This higher level control works by providing the reference of the reactive power Q^* into the converter control system. Previous research has shown the use of artificial neural networks implemented into grid feeding controllers such as in [39] and [40]. The ANN-based controller developed in [41] works for a grid-feeding converter of a residential solar PV system and controls the *d-q* reference into the control system. Fig. 5 shows a diagram of how the ANN developed for this paper would be implemented into the converter control system. The control diagram, adapted from [38], is for a three-phase system, but can easily be implemented in single-phase. The implementation of the controller is outside the scope of this paper and is considered in future research.

C. Regression Benchmark

The regression model used as a benchmark is the regression tree from the MATLAB Statistics and Machine Learning toolbox. The regression tree model is a type of decision tree, which is one of the most widely used machine learning techniques [37]. Depending on the inputs, a particular path will be taken down the tree resulting in the predicted output. Regression was used as a benchmark to compare with the results in [16].

V. Simulation Results

A. Performance metrics

The metrics used to compare the performance of ANNs to regression are mean average percentage error (MAPE) and R^2, also called goodness-of-fit.

$$MAPE = \frac{1}{N_s}\sum_{i=1}^{N_s}\frac{y_i - \hat{y_i}}{y_i}\cdot 100 \tag{8}$$

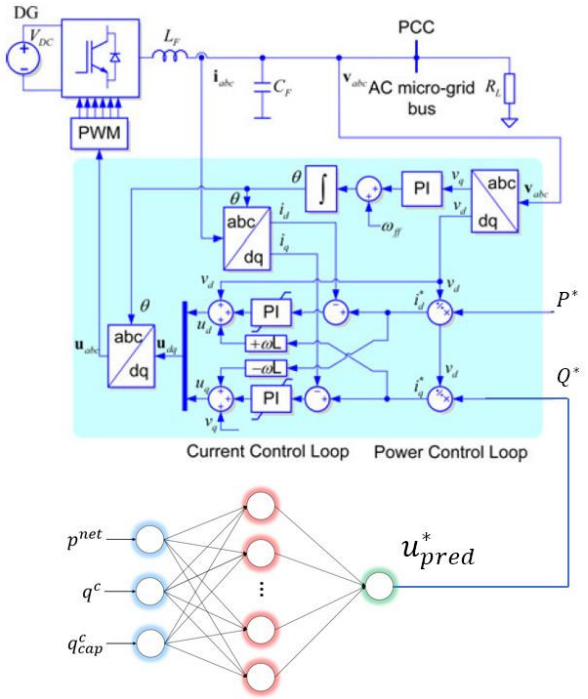

Fig. 5. ANN grid-feeding converter controller diagram

$$R^2 = 1 - \frac{\sum(y_i - \hat{y_i})^2}{\sum(y_i - \bar{y})^2} \tag{9}$$

where, N_s equals the number of scenarios, y_i equals the actual set-point on the test day, $\hat{y_i}$ equals the predicted set-point, and $\bar{y_i}$ equals the mean of the actual set-point.

B. Prediction results

Prediction results are obtained for each of the five PV inverter nodes for each of the five training scenarios. The performance metrics are calculated on each set of results. Each performance metric is averaged for all the five nodes in the network. The summarized version of the results is provided in Table I. Overall the ANN showed improvement in terms of the averaged MAPE and R^2 for all the scenarios over the regression based controller.

C. Z-bus and voltage profile results

The u^*_{pred} from ANN and regression are projected back again to their feasible set and are used to solve for the voltages satisfying the nonlinear power flows using the Z-bus method [27]. For each scenario, the average thermal loss with reactive power support from the PV inverter is compared to the case where inverters are not allowed to inject reactive power ($\mathbf{q}^{\mathrm{PV}} = 0$) and reported as percentage improvement. These results are summarized in Table II. Scenario 1 showed the greatest improvement in terms of grid losses for the ANN. This is likely due to the fact that it is a same year prediction. Scenario 4 showed good improvement as well in terms of grid losses for the ANN, which could be explained by the predictability of weekday data. Scenario 5, on the other hand,

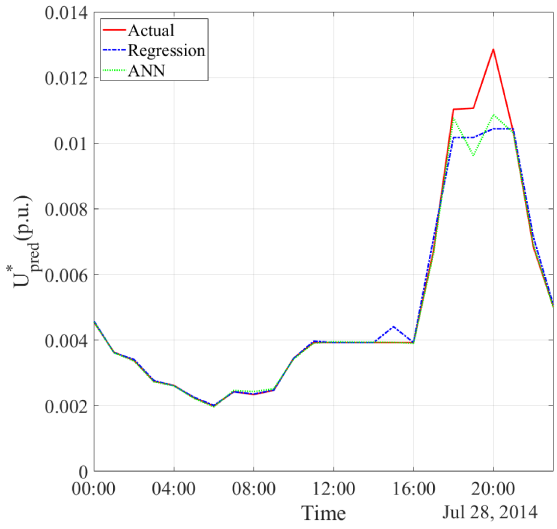

Fig. 6. Prediction Comparison - Scenario 1 - Node 646

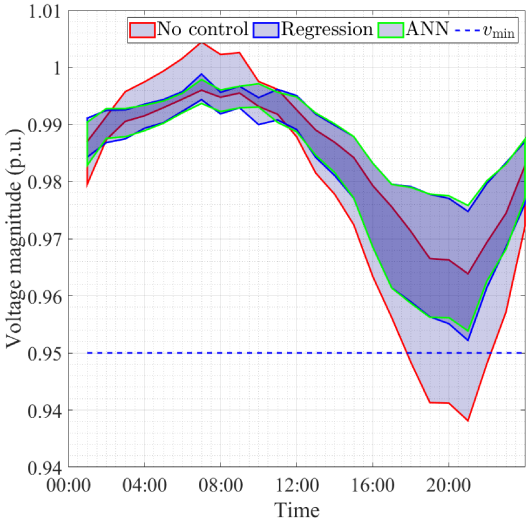

Fig. 7. Voltage Profile - Scenario 1

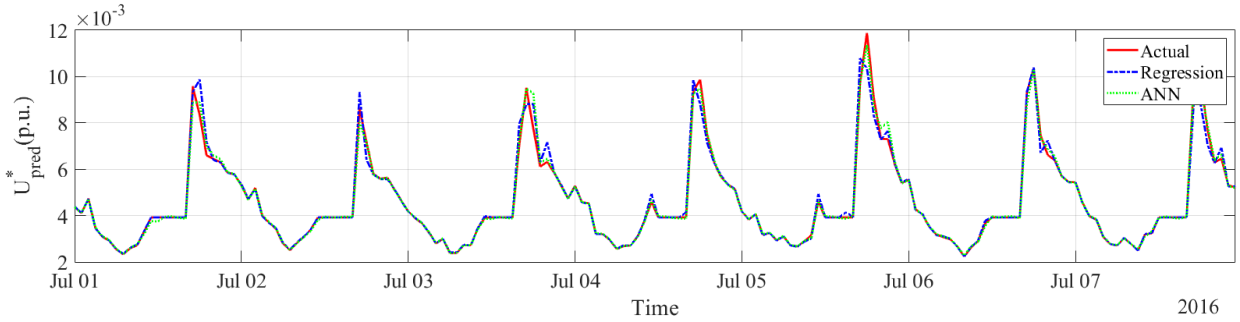

Fig. 8. Prediction Comparison - Scenario 3 - Node 646

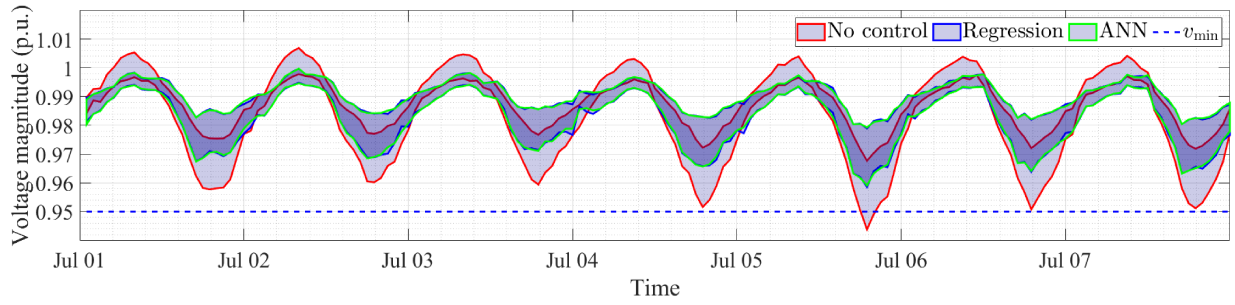

Fig. 9. Voltage Profile - Scenario 3

TABLE I

COMPARISON FOR AVERAGED PERFORMANCE METRICS

	Scenario - 1			Scenario - 2			Scenario - 3			Scenario - 4			Scenario - 5		
	MAPE	R-sqr	Time	MAPE	R-sqr	Time	MAPE	R-sqr	Time	MAPE	R-sqr	Time	MAPE	R-sqr	Time
Reg.	0.370	0.922	0.04	2.506	0.918	0.04	2.560	0.912	0.06	0.57	0.883	0.05	0.496	0.896	0.04
ANN	0.282	0.942	0.14	1.809	0.934	0.14	1.277	0.931	0.16	0.522	0.904	0.14	0.459	0.913	0.13

TABLE II

COMPARISON FOR PERCENTAGE IMPROVEMENT IN AVERAGE LOSSES

Scenario - 1			Scenario - 2			Scenario - 3			Scenario - 4			Scenario - 5		
Reg.	ANN	% Imp.	Reg.	ANN	% Imp.	Reg.	ANN	% Imp.	Reg.	ANN	% Imp.	Reg.	ANN	% Imp.
6.44	6.52	1.24%	5.35	5.35	0.00%	5.38	5.39	0.19%	5.26	5.29	0.57%	5.11	5.11	0.00%

having a smaller amount of weekend data, which is more variable in nature, lead to zero percent improvement in terms of grid losses over regression.

D. Plots for scenarios 1 and 3

The prediction for scenario 1 of the control input at node 646 is depicted in Figure 6. It can be seen the predictions are similar, but the MAPE and R^2 values are 0.02 and 0.97, respectively, for the ANN prediction, while the MAPE and R^2 values are 0.02 and 0.96, respectively, for the regression prediction. The voltage profile for scenario 1 can be seen in Fig. 7. The ANN is producing a tighter regulation on the voltage, particularly when the under-voltage occurs with the no-control case. The average losses for this scenario show a 1.24% improvement compared to regression.

The first week of predictions for scenario 3 can be seen in Fig. 8. The MAPE and R^2 values are 0.01 and 0.98, respectively, for the ANN prediction, and the MAPE and R^2 values are 0.01 and 0.97, respectively, for the regression prediction. The voltage profile can be seen in Fig. 9. The average losses for this scenario show a 0.19% improvement compared to regression.

VI. Conclusion and Future Work

This paper presents an ANN based controller that has proven to be more effective at prediction and voltage regulation compared to a benchmark of regression-based control. Overall, the ANN saw an improvement for the averaged MAPE and R^2 in all the training scenarios. Additionally, the ANN resulted in improvement in terms of grid losses for scenarios 1, 3 and 4. Future directions of research include scaling up to larger networks, such as the IEEE-123 bus feeder, and using a finer granularity of data, such as 15-minute or 1-minute. Another direction is simulating the ANN grid-feeding converter controller in a distribution network in OPAL-RT real-time simulator. Lastly, due to the data-driven nature of the problem, it is also worth investigating the impact of cyber attacks, and how to respond to false data injected into the system, which can cause disruption to the distribution network.

References

[1] M. Farivar, C. R. Clarke, S. H. Low, and K. M. Chandy, "Inverter var control for distribution systems with renewables," in *Proc. IEEE Int. Conf. on Smart Grid Communications (SmartGridComm)*, Oct. 2011, pp. 457–462.

[2] IEEE PES Industry Technical Support Task Force, "Impact of IEEE 1547 standard on smart inverter," May. 2018.

[3] W. Lin and E. Bitar, "Decentralized stochastic control of distributed energy resources," *IEEE Transactions on Power Systems*, vol. 33, no. 1, pp. 888–900, Jan. 2018.

[4] R. A. Jabr, "Linear decision rules for control of reactive power by distributed photovoltaic generators," *IEEE Transactions on Power Systems*, vol. 33, no. 2, pp. 2165–2174, Mar. 2018.

[5] M. Bazrafshan and N. Gatsis, "Decentralized stochastic optimal power flow in radial networks with distributed generation," *IEEE Transactions on Smart Grid*, vol. 8, no. 2, pp. 787–801, Mar. 2017.

[6] K. Turitsyn, P. Sulc, S. Backhaus, and M. Chertkov, "Options for control of reactive power by distributed photovoltaic generators," *Proceedings of the IEEE*, vol. 99, no. 6, pp. 1063–1073, Jun. 2011.

[7] S. Bolognani and S. Zampieri, "A distributed control strategy for reactive power compensation in smart microgrids," *IEEE Transactions on Automatic Control*, vol. 58, no. 11, pp. 2818–2833, Nov. 2013.

[8] B. Zhang, A. Y. S. Lam, A. D. Domnguez-Garca, and D. Tse, "An optimal and distributed method for voltage regulation in power distribution systems," *IEEE Transactions on Power Systems*, vol. 30, no. 4, pp. 1714–1726, Jul. 2015.

[9] K. S. Ayyagari, N. Gatsis, and A. F. Taha, "Chance constrained optimization of distributed energy resources via affine policies," in *Proc. IEEE Global Conf. on Signal and Information Processing*, Montréal, Canada, Nov. 2017.

[10] B. Zhang, A. D. Domnguez-Garca, and D. Tse, "A local control approach to voltage regulation in distribution networks," in *2013 North American Power Symposium (NAPS)*, Sep. 2013, pp. 1–6.

[11] N. Gatsis, L. Yalamanchili, M. Bazrafshan, and P. Risbud, "Decentralized coordination of energy resources in electricity distribution networks," in *Proc. IEEE Int. Conf. on Acoustics, Speech and Signal Processing*, Shanghai, China, Mar. 2016, pp. 3471–3475.

[12] N. Li, G. Qu, and M. Dahleh, "Real-time decentralized voltage control in distribution networks," in *Proc. 52nd Annual Allerton Conf. on Communication, Control, and Computing (Allerton)*. IEEE, 2014, pp. 582–588.

[13] F. McLoughlin, A. Duffy, and M. Conlon, "A clustering approach to domestic electricity load profile characterisation using smart metering data," *Applied Energy*, vol. 141, pp. 190 – 199, 2015. [Online]. Available: http://www.sciencedirect.com/science/article/pii/S0306261914012963

[14] R. Mieth and Y. Dvorkin, "Data-driven distributionally robust optimal power flow for distribution systems," *IEEE Control Systems Letters*, vol. 2, no. 3, pp. 363–368, Jul. 2018.

[15] O. Sondermeijer, R. Dobbe, D. Arnold, C. Tomlin, and T. Keviczky, "Regression-based inverter control for decentralized optimal power flow and voltage regulation," in *Proc. IEEE PES General Meeting*, Boston, MA, Jul. 2016.

[16] R. Dobbe, O. Sondermeijer, D. Fridovich-Keil, D. Arnold, D. Callaway, and C. Tomlin, "Data-driven decentralized optimal power flow," 2018.

[17] S. Karagiannopoulos, P. Aristidou, A. Ulbig, S. Koch, and G. Hug, "Optimal planning of distribution grids considering active power curtailment and reactive power control," in *IEEE Power and Energy Society General Meeting (PESGM)*, Jul. 2016, pp. 1–5.

[18] A. Garg, M. Jalali, V. Kekatos, and N. Gatsis, "Kernel-based learning for smart inverter control," in *Proc. IEEE Global Conf. on Signal and Information Processing*, Anaheim, CA, Nov. 2018.

[19] H. Xu, A. D. Domnguez-Garca, and P. W. Sauer, "A data-driven voltage control framework for power distribution systems," in *IEEE Power Energy Society General Meeting (PESGM)*, Aug. 2018, pp. 1–5.

[20] M. Jalali, V. Kekatos, N. Gatsis, and D. Deka, "Designing reactive power control rules for smart inverters using support vector machines," *arXiv preprint arXiv:1903.01016*, 2019.

[21] Q. Yang, G. Wang, A. Sadeghi, G. B. Giannakis, and J. Sun, "Real-time voltage control using deep reinforcement learning," *CoRR*, vol. abs/1904.09374, 2019. [Online]. Available: http://arxiv.org/abs/1904.09374

[22] K. S. Ayyagari, N. Gatsis, A. F. Taha, and B. Dong, "On static and adaptive policies for chance-constrained voltage regulation," in *Proc. Annual Asilomar Conference on Signals, Systems, and Computers*, Pacific Grove, CA, Oct. 2018.

[23] M. Bazrafshan and N. Gatsis, "Voltage regulation in electricity distribution networks using the conditional value-at-risk," in *Proc. IEEE Global Conf. on Signal and Information Processing*, Atlanta, GA, Dec. 2014, pp. 909–913.

[24] K. Baker, E. Dall'Anese, and T. Summers, "Distribution-agnostic stochastic optimal power flow for distribution grids," in *Proc. North American Power Symposium*, Denver, CO, Sep. 2016, pp. 1–6.

[25] E. DallAnese, K. Baker, and T. Summers, "Chance-constrained AC optimal power flow for distribution systems with renewables," *IEEE Transactions on Power Systems*, vol. 32, no. 5, pp. 3427–3438, Sep. 2017.

[26] C. M. Bishop, *Pattern recognition and machine learning, 5th Edition*, ser. Information science and statistics. Springer, 2007. [Online]. Available: http://www.worldcat.org/oclc/71008143

[27] M. Bazrafshan and N. Gatsis, "Comprehensive modeling of three-phase distribution systems via the bus admittance matrix," *IEEE Transactions on Power Systems*, vol. 33, no. 2, pp. 2015–2029, Mar. 2018.

[28] M. Baran and F. F. Wu, "Optimal sizing of capacitors placed on a radial

distribution system," *IEEE Transactions on Power Delivery*, vol. 4, no. 1, pp. 735–743, Jan. 1989.
[29] V. Kekatos, L. Zhang, G. B. Giannakis, and R. Baldick, "Fast localized voltage regulation in single-phase distribution grids," in *Proc. IEEE Int. Conf. on Smart Grid Communications*, Nov. 2015, pp. 725–730.
[30] A. Hassan, Y. Dvorkin, D. Deka, and M. Chertkov, "Chance-constrained ADMM approach for decentralized control of distributed energy resources," in *Proc. Power Systems Computation Conf.*, Dublin, Ireland, Jun. 2018, pp. 1–7.
[31] Y. Guo, K. Baker, E. Dall'Anese, Z. Hu, and T. Summers, "Data-based distributionally robust stochastic optimal power flow, Part II: Case studies," *IEEE Transactions on Power Systems*, to be published.
[32] R. T. Rockafellar and S. Uryasev, "Optimization of conditional value-at-risk," *Journal of Risk*, vol. 2, pp. 21–41, 2000.
[33] W. H. Kersting, "Radial distribution test feeders," *IEEE Transactions on Power Systems*, vol. 6, no. 3, pp. 975–985, Aug. 1991.
[34] O. Sondermeijer, "Regression-based inverter control for power flow and voltage regulation," Master's thesis, Delft University of Technology, The Netherlands, 2015. [Online]. Available: https://repository.tudelft.nl/islandora/object/uuid:4535a9a5-6928-42c0.../download
[35] "Pecan street dataport inc," https://dataport.cloud/.
[36] M. Grant and S. Boyd, "CVX: Matlab software for disciplined convex programming, version 2.1," http://cvxr.com/cvx, Mar. 2014.
[37] Y. R. M.W. Ahmad, M. Mourshed, "Trees vs neurons: Comparison between random forest and ann for high-resolution prediction of building energy consumption," *Energy and Buildings*, vol. 147, pp. 77–89, Oct. 2016.
[38] J. Rocabert, A. Luna, F. Blaabjerg, and P. Rodrguez, "Control of power converters in ac microgrids," *IEEE Transactions on Power Electronics*, vol. 27, no. 11, pp. 4734–4749, Nov. 2012.
[39] S. Li, M. Fairbank, C. Johnson, D. C. Wunsch, E. Alonso, and J. L. Proao, "Artificial neural networks for control of a grid-connected rectifier/inverter under disturbance, dynamic and power converter switching conditions," *IEEE Transactions on Neural Networks and Learning Systems*, vol. 25, no. 4, pp. 738–750, Apr. 2014.
[40] Xingang Fu and Shuhui Li, "Training recurrent neural network vector controller for inner current-loop control of doubly fed induction generator," in *2015 IEEE Power Energy Society General Meeting*, Jul. 2015, pp. 1–5.
[41] Y. Sun, S. Li, B. Lin, X. Fu, M. Ramezani, and I. Jaithwa, "Artificial neural network for control and grid integration of residential solar photovoltaic systems," *IEEE Transactions on Sustainable Energy*, vol. 8, no. 4, pp. 1484–1495, Oct. 2017.